Northumbria Research Link

Northumbria
University
NEWCASTLE

An Improved Direct Torque Control for a Single-Winding Bearingless Switched Reluctance Motor

Zhenyang Hao, Qiang Yu, Xin Cao, *Member, IEEE*, Xu Deng, Xiang Shen

***Abstract*—The direct torque control (DTC) and direct force control (DFC) method were introduced to reduce the torque and levitation force ripple in single-winding bearingless switched reluctance motors (SWBSRMs). However, it still has some disadvantages. Firstly, the flux-linkage control is not suitable for the DTC method in SWBSRMs. On the one hand, it can increase the torque ripple. On the other hand, the RMS current can be increased and then the torque-ampere ratio is decreased. Secondly, the vectors selection is also unreasonable, which can increase the torque ripple further. In order to solve these problems, an improved control method based on DTC and DFC method for SWBSRMs is proposed in this paper, which can obtain high torque-ampere ratio and low torque ripple simultaneously. In the proposed method, the flux-linkage loop control is not needed and the space voltage vector table is improved. The experimental results show that the torque ripple is reduced by 66.7%, the torque-ampere ratio is increased by 200% and the switching times in one electrical period are reduced by 47.3%.**

***Index Terms*—single-winding bearingless switched reluctance motor, direct torque control, direct force control, torque ripple, torque-ampere ratio.**

NOMENCLATURE

θ	Rotor angular position.
θ_{sr}	Angle between stator and rotor flux linkage.
i_{a1}-i_{a4}	Winding currents of phase A in BSRMs.
T_a	Instantaneous torque of phase A.
F_α , F_β	Radial forces on the direction of α-axis and β-axis, respectively.
p_0	Number of rotor poles.
L_m	Mutual inductance.
L_s , L_r	Stator and rotor inductances amplitude, respectively.
Ψ_s ,Ψ_r	Stator and rotor flux-linkage amplitude, respectively.
σ	Leakage inductance coefficient.
i_s	Current of stator winding in SRMs.
c	Constant 1.01.
h	Lamination length of the iron core.
l_0	Air-gap length between the stator and rotor poles.
N_s	Number of winding turns.
r	Radius of rotor.
μ_0	Permeability of vacuum.

Manuscript received . This work was supported by the National Natural Science Foundation of China, under Grant No. 51877107, 51577087 and 51477074. (*Corresponding author: Xin Cao*.)

Zhenyang Hao, Qiang Yu and Xin Cao are with the Department of Electrical Engineering and also with the Center for More-Electric-Aircraft Power System, Nanjing University of Aeronautics and Astronautics, Nanjing 211106, China (e-mail: zhenyang_hao@nuaa.edu.cn; yuqiang@nuaa.edu.cn caoxin@nuaa.edu.cn).

Xu Deng is with School of Engineering, Newcastle University, Newcastle upon Tyne NE1 7RU, U.K. (e-mail: xu.deng@ncl.ac.uk).

Xiang Shen is with Department of Mechanical and Construction Engineering, Northumbria University, Newcastle upon Tyne NE1 8ST, U.K. (e-mail: x.shen@outlook.com).

I. INTRODUCTION

IN last decades, switched reluctance motors (SRMs) have obtained more and more attention from the worldwide industry due to its particular characteristics with centralized windings mounted on stator poles and no winding or permanent magnets on rotor pole [1-2]. Therefore, SRMs have the advantages of robust structure, low cost and great fault–tolerance capability [3-4]. However, some shortcomings also restrict its application, such as large torque ripple, vibration, noise, etc., which makes SRMs impossible to be used in high-speed applications [5-6].

In order to solve these problems above, scholars from different countries have focused on SRMs. Recently, bearingless motor technology is developed gradually due to its advantages of no friction between the mechanical bearing and rotor shaft. Thus, motors can operate under the high-speed application by utilizing bearingless motor technology. Based on these superiorities, bearingless switched reluctance motor (BSRM) is proposed accordingly, which can make the rotor rotate and levitate at the same time [7-9]. Then the friction between mechanical bearing and rotor shaft can be reduced obviously and the motor can obtain higher speed.

According to the number of windings on the stator poles, BSRMs can be divided into two types, i.e. dual-winding BSRMs and single-winding BSRMs. Dual-winding BSRMs were firstly proposed in the 1990s by Japanese scholars. There are two windings mounted on each stator pole. One is called main winding, which is used to generate a bias magnetic field. The other is called levitation winding, which is utilized to unbalance the original magnetic field to obtain the levitation force [10-12]. After that, single-winding BSRMs were proposed to simplify the winding configuration [13-15]. There is only one winding on each stator pole, and the torque and

levitation force are controlled by adjusting each winding current only, thus the current algorithm should be designed reasonably.

There are two control objects in BSRMs, i.e. torque and levitation force. In [16], the average torque and instantaneous levitation force are controlled. The torque is regulated by square-wave current and advanced angle. The levitation current is calculated by the reference levitation force, square-wave current and rotor angular position. This method makes the shaft rotate and levitate smoothly. In order to achieve the decoupling of torque and levitation force, an independent control strategy is proposed in [17]. The current-conduction region is extended to the negative-torque region in this method, which makes the average torque zero in the levitation region. Therefore, this strategy can regulate the torque and levitation force independently. However, the control strategies above are based on winding current, and there still exist large torque and levitation force ripple, which is not beneficial to motor operation.

Afterwards, owing to the superiority of direct torque control (DTC) method for SRMs, an advanced method named DTC and direct force control (DFC) for BSRMs was proposed accordingly [18-19]. The torque and levitation force are selected as control objects, and the hysteresis-loop controller is adopted to make the torque and levitation force controlled within the hysteresis-loop width [20-21]. However, the winding current is conducted in the negative-torque region, which reduces the total output torque. Then the effective value of current will increase and torque-ampere ratio will decrease. In [22], another control strategy named direct instantaneous torque control (DITC) was developed. This strategy takes the instantaneous torque as the control object and adopts the hysteresis-loop controller as well.

In order to reduce the negative torque generated and increase the torque-ampere ratio in single-winding BSRMs, this paper develops an improved method based on direct torque control (DTC). Different from the conventional DTC method in [18], this method removes the flux-linkage loop control and improves the space voltage vector table to make vectors allocation more reasonable.

The rest of paper is organized as follows. Firstly, the levitation principle of SWBSRMs and mathematical models are illustrated in Section II-A. Secondly, the conventional DTC and DFC method is introduced briefly in Section II-B. Moreover, the improved voltage vector tables and the principle of vector selection are also demonstrated in Section II. After that, the implementation procedures and control block are also presented. The simulation and experimental results are shown in Section III and the conclusions are made in Section IV.

II. Proposed Method For SWBSRM

A. Operation Principle of SWBSRMs

As shown in Fig. 1, the structure of the single-winding BSRMs are identical to that of the conventional SRMs. It consists of twelve stator poles and eight rotor poles. Only one excitation winding is embedded on each stator pole and there are no windings on rotor poles. For example, four coils of phase A are conducted with different currents, which can produce different magnetic flux density in four air gaps. If the magnetic flux density in air-gap 1 is larger than that in air-gap 3, the radial force can be generated along the positive direction of α-axis. Similarly, if the magnetic flux density in air-gap 2 is larger than that in air-gap 4, the radial force can be generated along the positive direction of the β-axis. The principle of levitation force generated by phases B and C is the same as that of phase A. Differently, due to the location of phases B and C, the force of two phases should be transformed into a coordinate system of phase A. Therefore, radial forces towards any directions can be obtained by regulating four coil currents of per phase.

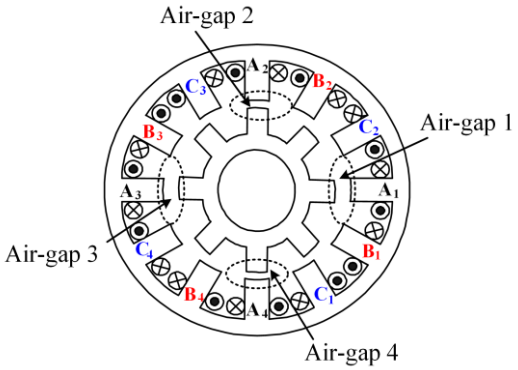

Fig. 1. The structure of 12/8 SWBSRM.

In a single-winding BSRM, there are two control objects, i.e. torque and levitation force. Stable torque makes rotor rotate continuously and stable levitation force makes the rotor suspend smoothly. Hence, in order to analyze the relationship between two variables reasonable, the accurate mathematical models of them are necessary. The virtual-work method is adopted to establish the models below.

Assuming that the influences of leakage inductance and magnetic saturation are ignored. The expressions of torque and levitation force with regard to four coil currents of each phase are obtained in [23]. Due to four coil currents in the expressions, it will increase the difficulty of control certainly. Therefore, taking phase A as an example, four coil currents of phase A can be simplified as

$$i_a^*=(i_{a1}+i_{a3})/2=(i_{a2}+i_{a4})/2, \tag{1}$$

$$\Delta i_{a1}=|i_{a1}-i_{a3}|/2, \tag{2}$$

$$\Delta i_{a2}=|i_{a2}-i_{a4}|/2. \tag{3}$$

Where, i_a^* is the average excitation current of phase A, Δi_{a1} and Δi_{a2} are current difference along α-axis and β-axis respectively. As derived in [23], the expressions of torque and levitation force can be written as

$$T_a=J_t(\theta)\left(2i_a^{*2}+\Delta i_{a1}^2+\Delta i_{a2}^2\right), \tag{4}$$

$$F_\alpha=4K_f\left(\theta\right)i_a^*\Delta i_{a1}, \tag{5}$$

$$F_\beta=4K_f\left(\theta\right)i_a^*\Delta i_{a2}. \tag{6}$$

Where, the torque coefficient $J_t(\theta)$ and levitation force

coefficient $K_f(\theta)$ can be expressed as

$$J_t(\theta) = \begin{cases} N_s^2\left(\dfrac{\mu_0 hr}{l_0} - \dfrac{16\mu_0 chr}{\pi\left(\pi l_0 - 4cr\theta\right)}\right), & when\ \theta \in \left[-\dfrac{\pi}{12}, 0\right], \\ -N_s^2\left(\dfrac{\mu_0 hr}{l_0} + \dfrac{16\mu_0 chr}{\pi\left(\pi l_0 + 4cr\theta\right)}\right), & when\ \theta \in \left[0, \dfrac{\pi}{12}\right]. \end{cases}$$

$$K_f(\theta) = \frac{\mu_0 hrN_s^2\left(\pi - 12|\theta|\right)}{24l_0^2} + \frac{8\mu_0 hrcN_s^2|\theta|}{\pi\left(\pi l_0^2 + 4cr|\theta| l_0\right)}.$$

B. Conventional DTC and DFC Method Compared in this Paper

In order to reduce the torque and levitation force ripple, a simple method called direct torque control (DTC) and direct force control (DFC) was proposed in [19]. DTC method in SWBSRMs is similar to that in conventional SRMs, as shown in Fig. 2. This method divides an electric angle of the rotor into six sectors, i.e. N=1~6. There is only one space voltage vector in each sector. Six voltage vectors v_1~v_6 are defined as three kinds of different voltage states, as shown in Fig. 3. State "1" represents that two switches Q_1, Q_2 both turn on, and the winding voltage is equal to bus voltage $+U_{dc}$; State "0" represents that Q_2 turns on and Q_1 turns off, and the winding voltage is zero. State "-1" means that two switches Q_1, Q_2 both turn off, and the winding voltage is $-U_{dc}$.

Similarly, the control objects of DTC for SWBSRM are torque and magnetic flux as well. Three-phase composed magnetic flux is firstly calculated by voltage vectors, then it should be transformed into the α-β reference frame. Finally, the amplitude and angle of magnetic flux can be obtained as [19]. The sector is determined by magnetic flux angle δ. The specific selection process of voltage vectors was demonstrated in [19].

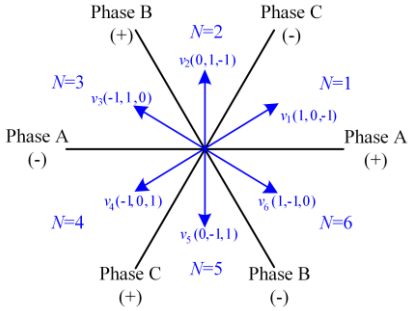

Fig. 2. Definition of space voltage vectors in SWBSRMs.

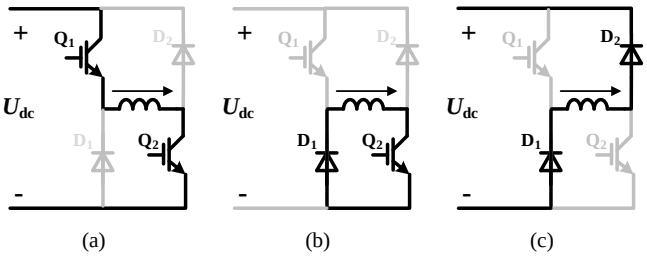

Fig. 3. Switching states of power converter:(a) "+". (b) "0". (c) "-".

Due to separate excitation of four coils on each phase poles, the voltage vector should be distributed into each coil. Because the levitation coefficient is large in the inductance region [-7.5 °, 7.5 °], the control region for DFC can be selected in this region. The equivalent voltage vector for DTC and DFC in SWBSRMs is illustrated in Fig. 4. The different equivalent vectors of each phase refer to different switching states [19]. It is worth noting that four poles voltage symbols of each phase must be equal to the original phase voltage symbol after being combined.

The principle of composition is shown in Table I. For example, if the voltage vector of three phases is determined as v_6 (1, -1, 0) according to DTC, and phase A needs to provide the levitation force now, then the switching state of phase A can be split into many states. When the required levitation force is along the positive direction of α-axis or β-axis, i.e. $F_\alpha > 0$ or $F_\beta > 0$, the switching state of phase A is defined as (1, 1, 0, 0). Since phases B and C are not needed to provide levitation forces in this region, their switching states of four coils keep the same with their original voltage vectors. Therefore, v_6 (1, -1, 0) can be transformed to ((1, 1, 0, 0), (-1, -1, -1, -1), (0, 0, 0, 0)). Similarly, other three-phase voltage vectors can also follow the above procedures.

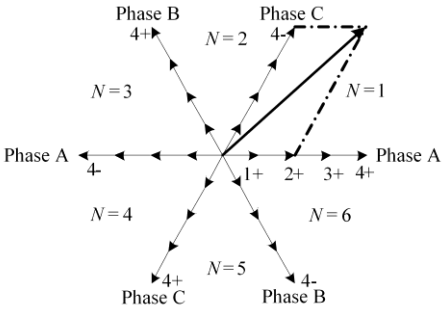

Fig. 4. Equivalent voltage vector for DTC and DFC in SWBSRMs.

TABLE I
ADDITION RULE FOR SWITCHING STATES

Addition	1,1	1,-1	1,0	-1,-1	-1,0	0,0
Result	1	0	1	-1	-1	0

C. Removal of Flux-Linkage Loop

DTC method was firstly proposed and applied to Induction Motors (IMs) [24]. It can control the torque and flux-linkage amplitude respectively to simplify the implementation of the control algorithm. Then the DTC method is applied to permanent magnet synchronous motors (PMSMs) due to its particular advantages. According to electromechanical energy conversion, the generated motor torque can be expressed as

$$T_e = p_0 \frac{L_m}{\sigma L_s L_r}|\psi_s||\psi_r|\sin\theta_{sr} \quad . \tag{7}$$

Where, p_0 represents the poles number; L_m represents the mutual inductance; L_s and L_r represent the stator and rotor inductances respectively; σ represents the leakage inductance coefficient; $|\Psi_s|$ and $|\Psi_r|$ represent the stator and rotor flux-linkage amplitude respectively; θ_{sr} represents the angle between stator and rotor flux linkage. From (7), the electromagnetic torque is related to the stator, rotor flux-linkage amplitude and their phase angle. Two conclusions can be summarized as below:

(a) Flux linkage stability is the premise of torque stability;

(b) Torque increases as the flux angle increases between 0° to 90°.

On the one hand, in IMs, the varying speed of rotor flux linkage is much slower than that of stator flux linkage, thus the rotor flux linkage can be seen as constant in one control period. In PMSMs, the rotor flux-linkage amplitude is always the same because there are only permanent magnets and no windings on the rotor. Then the constant amplitude of stator flux-linkage ensures the constant torque. That is to say, the stator flux linkage must be controlled into a circle to guarantee the stability of the torque for IMs and PMSMs. On the other hand, the increase and decrease of torque depend on the angle θ which is between stator and rotor flux linkages. When the torque needs to be increased, just the flux angle θ is increased only. That means that it needs to increase the rotating speed of the stator flux linkage by implementing the reasonable vector.

However, the nature of generated torque in BSRMs is different from IMs and PMSMs. The torque produced in BSRMs and IMs are reluctance torque and electromagnetic torque respectively. Thus the torque can be simply written as

$$T_e \approx i_s \frac{\partial \psi_s(\theta, i_s)}{\partial \theta}. \quad (8)$$

Where, i_s represents the current of stator winding; $\Psi_s(\theta, i_s)$ represents stator flux linkage, which is related to rotor rotation angular and stator winding current. The torque in BSRMs is related to the movement velocity of stator flux linkage. Thus, the constant flux linkage amplitude is not necessary to keep the torque steady. In addition, the flux-linkage control can make the currents conducted in the inductance-descending region, and the torque-ampere ratio will be decreased. Finally, due to the addition of flux-linkage control, the motor has one more control object. Then the flux-linkage control can also disturb the selection of vectors, and the selected vector is not the best one to increase torque, which results in the increase of torque ripple. On the other hand, vectors can be changed continuously in the sector with the change of torque and flux-linkage. It results in the increase of the switching times as well, and then the switching loss is also increased.

Based on the analysis above, some disadvantages of the constant flux-linkage control in BSRMs can be listed as follows.

(a) Flux-linkage amplitude is not helpful for torque control of SRMs, and it will increase the burden of the processor.
(b) The current is conducted in the inductance descending region, which will increase the RMS current and decrease the torque-ampere ratio.
(c) The additional flux-linkage loop is a disturbance for the torque regulation, which can increase torque ripples.
(d) Finally, The flux linkage can also increase the switching times, which increases the switching loss.

In summary, the constant flux-linkage control is not necessary for DTC method in BSRMs. In order to simplify the control algorithm, it should be removed. Then the control object is torque only for DTC method in BSRMs.

D. Optimization of Voltage Vector for DTC method

The definition of original three-phase voltage vectors in BSRMs are shown in Fig. 2. These voltage vectors can regulate the produced torque steadily at the non-commutation moment, but they are not necessarily at the commutation moment. For example, when the stator-rotor relative position is shown in Fig. 5 shadowed part, the sector is turning from six to one, whose inductance curves are also shown in Fig. 6. The voltage vector is also changed from v_1 (1, 0, -1) to v_2 (0, 1, -1) and the voltage symbol of phase B turns from "0" to "1", which has two disadvantages. Firstly, when the rotor moves to sector five, the voltage symbol of phase B is "-1" according to the vectors table. Hence, "0" has no meaning to increase torque in sector six. Secondly, after the sector becomes one, the current of phase-B winding is increasing slowly from zero, which can result in commutation torque ripples. Therefore, v_1 (1, 0, -1) in sector six cannot produce the smallest torque ripple. Three-phase voltage vectors should be improved.

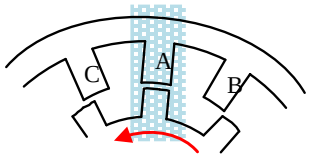

Fig. 5. Stator-rotor relative position.

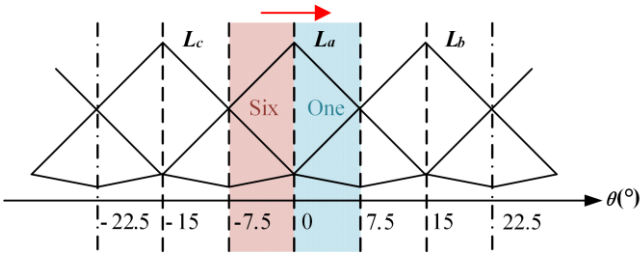

Fig. 6. Inductance curves of sector one and six.

Fig. 7 shows the definition of the improved voltage vectors for DTC method when torque increases. Six vectors without voltage symbol "0" are added to the original vectors compared with that in Fig. 2, which reduces the torque ripple. For example, when the rotor moves to the sector six, the voltage symbol of phase B should select "1". On the one hand, it increases torque slightly. More importantly, it can shape current to reduce the torque ripple when the rotor moves to sector one. Therefore, the vector should select v_8 (1, 1, -1), not v_1 (1, 0, -1). Then after the rotor moves into the sector one, if the levitation force is not considered, the phase-B winding should be excited to generate positive torque. Thus the voltage symbol should be "1". The two switches of phase-A winding should turn off to avoid the negative-torque generation, and its voltage symbol should be "-1" accordingly. The phase-C inductance is located in the first half of the bottom region, which cannot generate effective torque. Therefore, the voltage symbol of phase-C winding is "-1". According to the analysis above, the most suitable vector in Fig. 7 is v_9 (-1, 1, -1). In contrast, if taking the levitation force into account, the vector selection will have a little difference. The selection principle of phase B and C is the same as above because these two phases do not need to provide levitation force.

The phase-A inductance is located in the upper half of the descending region, which is one of the best regions to generate levitation force. It is also considered that the negative torque ought to be less. Hence the appropriate voltage symbol of phase A is "0". In summary, the most suitable vector considering the levitation force is v_2 (0, 1, -1). When the rotor moves to other sectors, the principle of vector selection is the same as well.

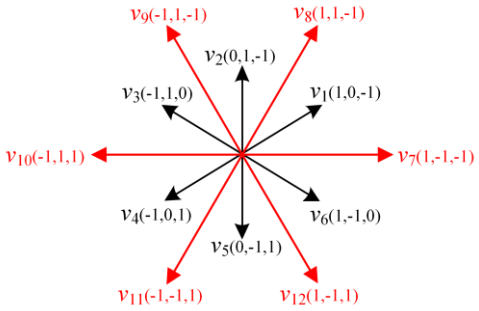

Fig. 7. Definition of the improved voltage vectors for DTC method when torque increases.

The DTC theory above is applicable to the case of torque increase. If the output torque needs to be decreased, there are two approaches to achieve it. On the one hand, two switches which belong to the phase in the inductance-ascending region can be turned off. Then the winding current flows through the two diodes. The voltage symbol is "-1" in this case. On the other hand, two switches which belong to the phase in the inductance-descending region can be turned on. Then current can flow through the winding to generate the negative torque, thus the average torque will be reduced. The voltage symbol is "1" in this case accordingly. Obviously, the second method is to reduce the torque by sacrificing the torque-ampere ratio. This method is not reasonable. In other words, the voltage symbol should not turn to "1" when the torque needs to be decreased. Based on this case, all the voltage vectors shown in Fig. 7 does not meet the requirement. The three-phase voltage vector table needs to be redesigned for the torque decrease.

Fig. 8 shows the definition of the improved voltage vectors for DTC when torque decreases. It adds $-v_0$ (-1, -1, -1) on the basis of the vector table for conventional SRMs [25]. For example, the rotor moves to the sector one. In SRMs, $-v_3$ (-1, 0, -1) can be selected to reduce the torque. However, this vector is not suitable for BSRMs because BSRMs need to consider the levitation force. The winding current cannot drop to zero during the upper half of the descending region. Therefore, the voltage symbol of phase A should select the voltage symbol "0" which makes current drop slowly, not "-1". At the same time, in order to make the torque decrease quickly, the voltage symbol of phase B also should select "-1". Then the three-phase voltage vector is $-v_1$ (0, -1, -1). The analysis is the same when the rotor rotates to other sectors. Fig. 9 shows the voltage-vector selection region for the proposed method and conventional DTC and DFC method. In order to reduce the negative torque, the current is shut off in the region of (-37.5 °, -22.5 °) with the proposed method. However, winding currents are conducted in full cycle with the conventional DTC and DFC method, which produces more negative torque.

Finally, the three-phase voltage vector selection rule for each sector can be obtained, as shown in Table II. The row of Table represents the sector symbol *N*, where *N* is the value from 1 to 6. The column represents the signal of torque increasing or decreasing. "T+" represents increasing torque and "T-" represents decreasing torque respectively. Besides, the selection of switching states for the proposed DTC and DFC method is shown in Table III. For example, if the levitation force is provided by phase-*k* winding at that time and the basic voltage vector of it is "1", and the direction of levitation force is "$F_\alpha > 0$, $F_\beta > 0$", then the switching states of phase-*k* winding can be transformed to (1, 1, 0, 0).

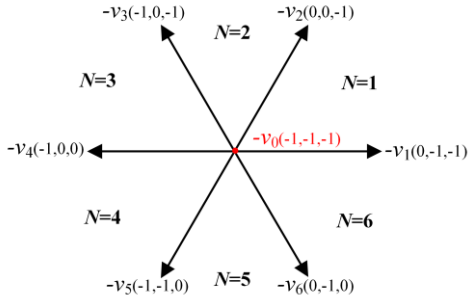

Fig. 8. Definition of the improved voltage vectors for DTC when torque decreases.

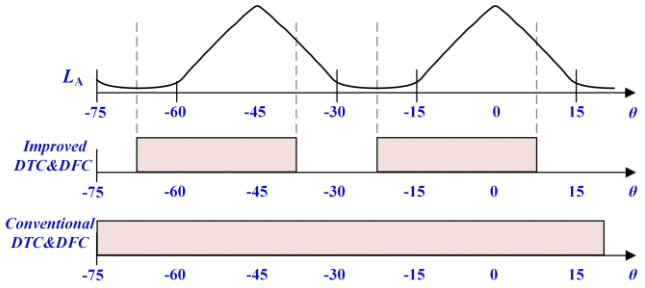

Fig. 9. Voltage-vector selection region for the proposed method and conventional DTC and DFC method.

TABLE II
VECTOR SELECTION RULE FOR PROPOSED DTC METHOD

Signal \ Sector *N*	1	2	3	4	5	6
T+	v_2	v_{10}	v_4	v_{12}	v_6	v_8
T-	$-v_1$	$-v_0$	$-v_3$	$-v_0$	$-v_5$	$-v_0$

E. Analysis of the torque with proposed method

In order to verify the analysis above, some FEM simulations are completed with the proposed method and conventional DTC and DFC method.

Fig. 10 shows the FEM results of the torque with different currents and rotor angles. The winding currents are conducted from 0.2A to 1A, and the rotor angle is from -22.5 °to 22.5 °. It can be seen that the torque is proportional to the square of current. In addition, the torque is positive when the region of rotor angle is (-15 °, 0 °), and torque is negative when the region of rotor angle is (0 °, 15 °). Fig. 11 shows the comparison of FEM results and calculation results of torque when the current is 0.4A. It can be seen that the calculation results through mathematical models are almost the same as FEM results, which proves the

TABLE III
SELECTION OF SWITCHING STATES FOR PROPOSED DTC AND DFC METHOD

Basic voltage vector	Direction of levitation force	Switching states
1	F_α>0 , F_β>0	(1, 1, 0, 0)
1	F_α>0 , F_β<0	(1, 0, 0, 1)
1	F_α<0 , F_β>0	(0, 1, 1, 0)
1	F_α<0 , F_β<0	(0, 0, 1, 1)
0	F_α>0 , F_β>0	(1, 1, -1, -1)
0	F_α>0 , F_β<0	(1, -1, -1, 1)
0	F_α<0 , F_β>0	(-1, 1, 1, -1)
0	F_α<0 , F_β<0	(-1, -1, 1, 1)
-1	F_α>0 , F_β>0	(0, 0, -1, -1)
-1	F_α>0 , F_β<0	(0, -1, -1, 0)
-1	F_α<0 , F_β>0	(-1, 0, 0, -1)
-1	F_α<0 , F_β<0	(-1, -1, 0, 0)

accuracy of the mathematical models in Subsection II-A.

Fig. 12 shows the comparison of phase-A torque with the conventional and proposed method by FEM. The current data of two methods is obtained by experimental waveforms, and then are imported to Ansoft. Finally, the phase torque curve produced by the corresponding currents is obtained. From Fig. 12, the positive and negative torques with the conventional method are both larger than that with the proposed method. This is because the RMS current of the conventional method is larger. However, the average torques with two methods are identical. Therefore, compared with the conventional method, the torque-ampere ratio with the proposed method is larger.

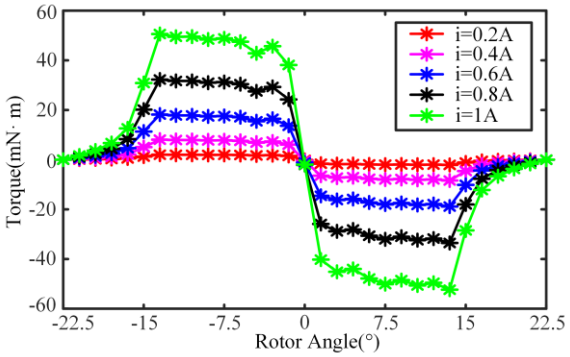

Fig. 10. FEM results on the torque with different currents and rotor angles.

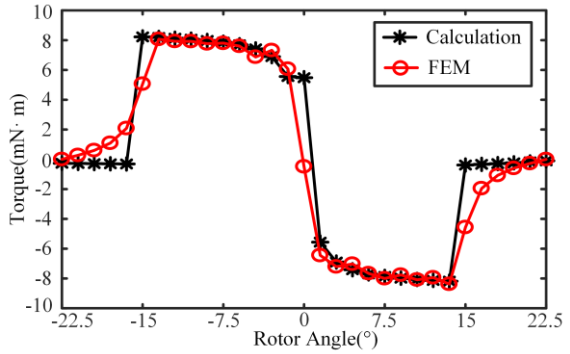

Fig. 11. Comparison of FEM results and calculation results of torque when the current is 0.4A.

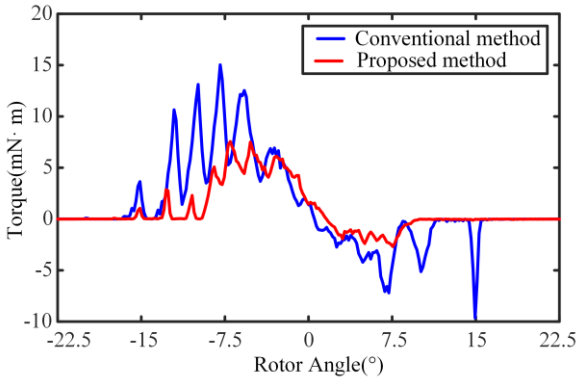

Fig. 12. Comparison of phase-A torque with the conventional and proposed methods by FEM.

F. Implementation of the Proposed Method

In single-winding BSRMs, when the windings on the two opposite poles are conducted with different currents, there will generate different magnetic-flux densities in the air gaps. The radial magnetic pull F_r can be illustrated as [19]

$$F_r = \frac{B^2 S}{2\mu_0}. \tag{9}$$

Where, B represents the air-gap flux density between stator and rotor poles; S represents the overlap area of stator and rotor poles. Besides, the air-gap flux density B can also be written as

$$B = \frac{\Psi}{NS} = \frac{Li}{NS}. \tag{10}$$

Where, Ψ represents the air-gap flux linkage; L represents the inductance of stator winding; i represents the current of stator winding. Then Substituting (10) into (9), (9) can also been written as

$$F_r = \frac{L^2}{2N^2\mu_0 S} i^2. \tag{11}$$

From (11), it can be seen that the radial magnetic pull F_r is proportional to the square of the winding current i. Therefore, in order to generate the levitation force along the certain direction, the stator pole windings on both sides of that direction should be conducted with different currents. Then the radial force along any certain direction can be expressed as

$$F_{rx} = \frac{L^2}{2N^2\mu_0 S}\left(i_{rx1}^{\ 2} - i_{rx3}^{\ 2}\right). \tag{12}$$

Where, F_{rx} represents the radial magnetic pull along any certain direction; i_{rx1} and i_{rx3} represent the two pole windings currents on both sides along that direction. Thus, three-phase voltage vector should also be assigned to each pole coil through the DFC method after it is achieved.

The principle of DFC for the proposed method is similar to that for the conventional method, which is illustrated in Subsection II-B. However, one point is worth to be noted. In the conventional DTC and DFC method, when the levitated phase is changed from one to another, its windings are conducted with currents. Due to the differences in hardware, four coil currents of the same phase cannot be the same exactly, then the extra levitation force will be generated. Contrarily, in the proposed

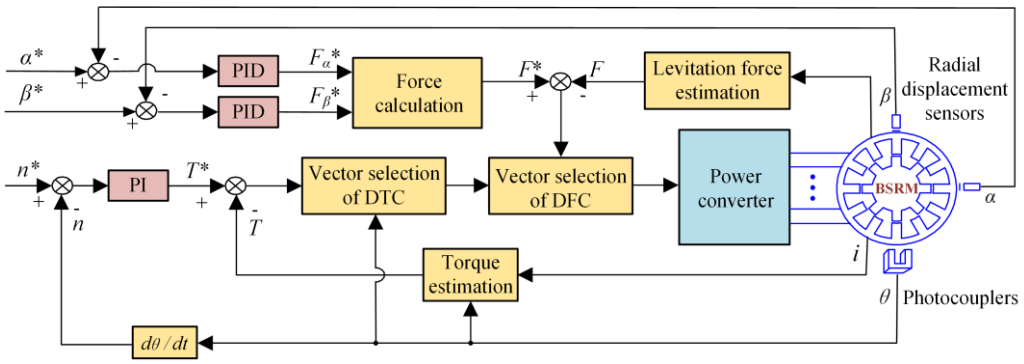

Fig. 13. Control block of the proposed method.

method, four coil currents can be dropped to zero in the phase commutation, which makes the levitation force generated by the previous phase become zero. Then the composed levitation force is generated only by one phase at any time. Therefore, levitation force can be controlled more stably. The specific implementation of the proposed method is concluded by three steps.

(a) Firstly, the real torque and levitation force are estimated respectively by (4) - (6). Then these hysteresis-loop outputs can be obtained by comparing the reference and the real values.

(b) Then the sector is determined by checking the rotor angular position. Three-phase voltage vectors are selected by the improved DTC method in Table II.

(c) Finally, the three-phase voltage vectors are assigned to each pole winding by the DFC method. The levitation force is produced by the phase which is located in [-7.5°, 7.5°]. Four winding-voltage symbols of that phase needs to satisfy the rule shown in Table I, and the others are consistent with their phases voltage symbols as well.

G. Control Block of the Proposed Method

Fig. 13 shows the control block of the proposed method. Firstly, the rotor angular position is measured by photocouplers and then the speed is calculated. The speed error is regulated by PI controller to obtain the reference torque. The real torque is estimated by currents and angular position. Afterwards, the three-phase voltage vectors are selected through the improved voltage vector table.

For the levitation control, the radial displacements along α- and β-axes are measured by eddy-current sensors. The given radial displacement values of α^* and β^* are always zero in experiments to ensure that the real radial displacements of shaft can be regulated around its geometric-center position. Then the levitation forces F_α^* and F_β^* are obtained by PID controllers. The real levitation force is estimated by currents and angular position as well. After that, the three-phase voltage vector is divided into four coils of each phase according to the principle of DFC. Finally, the switching symbols are obtained for the power converter to excite the motor.

III. Simulation and Experimental Results

In order to verify the performance of the proposed method, some simulations and experiments are carried out on a single-winding BSRM prototype. The parameters of the prototype are shown in Table IV. The picture of the prototype and its control circuits are shown in Fig. 14 (a). The control circuits include the three-phase power converters, DSP controller, CPLD controller, current and displacement sampling circuits, etc. Among them, the power converter of each phase adopts the asymmetric half-bridge circuit with four legs. The control algorithm is programmed in TI TMS320F2812 and Altera EPM1270. The current is sampled by hall sensors and scaled by regulation circuits, and then transferred to DSP. The displacement signals are sampled by four eddy-current sensors. The sensitivity of eddy-current sensors is 16V/mm. In addition, the rotor angular position is detected by three photocouplers, which can be used to calculate the motor speed.

The enlarged view of motor shaft and backup bearing are shown in Fig. 14 (b). The backup bearing is utilized to prevent collision between the stator and rotor. The average air-gap length between shaft and backup bearing is 200 μm, which is less than the average air-gap length between stator and rotor, i.e. 250 μm.

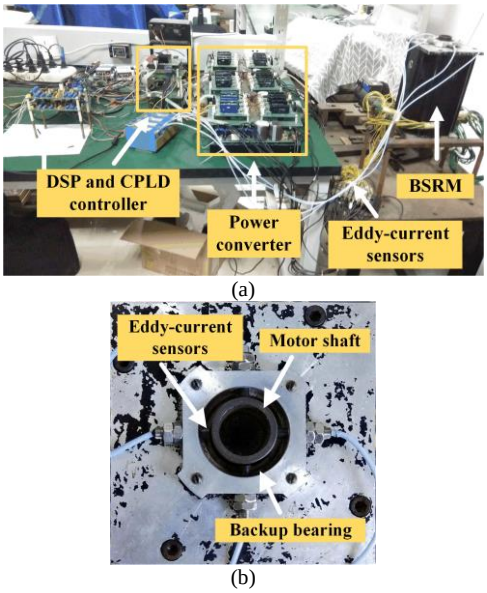

Fig. 14. Platform of experimental prototype: (a) Control circuits and motor. (b) Enlarged view of motor shaft and backup bearing.

TABLE IV
PARAMETERS OF PROTOTYPE

Parameters	Values
Number of stator poles	12
Number of rotor poles	8
Number of winding turns	60 turns
Rated power	0.5 kW
Rated current	5 A
Rated voltage of the motor	100 V
Rated average radial force	50 N
Arc angle of rotor and stator teeth	15 °
Outside diameter of stator core	123 mm
Inside diameter of stator pole	54 mm
Radius of rotor pole	26.75 mm
Stack length lamination	55 mm
Average air-gap length between rotor and stator	0.25 mm
Average air-gap length between shaft and backup bearing	0.2 mm

A. *Comparison of Simulation Results*

The system simulation models with the conventional DTC and DFC method and the proposed method have been built in Matlab/Simulink, respectively, to verify the demonstrated performance. The simulation parameters are listed in Table V.

TABLE V
SIMULATION PARAMETERS

Parameters	Values
Reference speed	1000 r/min
Load torque	1 N m
Radial force in α-axis	30 N
Radial force in β-axis	40 N

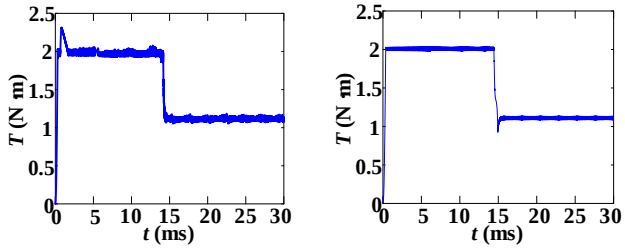

(a) (b)

Fig. 15. Simulation waveforms of torques: (a) Conventional DTC and DFC method. (b) Proposed method.

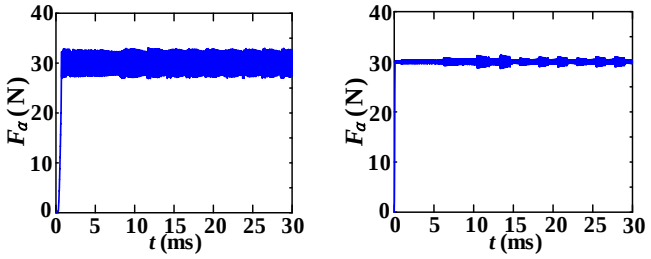

(a) (b)

Fig. 16. Simulation waveforms of levitation forces in α-axis: (a) Conventional DTC and DFC method. (b) Proposed method.

Fig. 15 shows the waveforms of torque with two different methods. Firstly, the electromagnetic torque reaches the limited value, i.e. 2 N m, the motor speed begins to increase. When the speed reaches 1000 r/min, the electromagnetic torque decrease to be equal to the load torque. The torque ripples of the two methods are 0.068N·m and 0.167N·m, respectively. Therefore, the simulation results show that the torque ripple in the proposed method is less than that in the conventional method.

Figs. 16 and 17 show the waveforms of levitation forces in α- and β-axes with the two methods. It can be seen that the levitation-force ripples in the proposed method are obviously less than that in the conventional method.

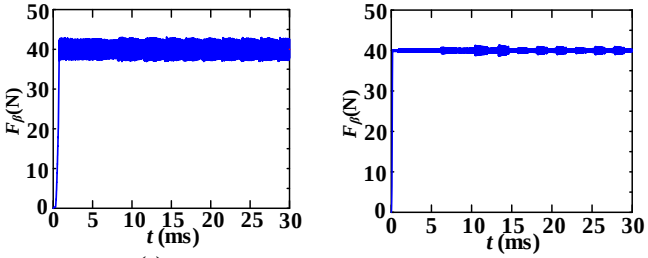

(a) (b)

Fig. 17. Simulation waveforms of levitation forces in β-axis: (a) Conventional DTC and DFC method. (b) Proposed method.

B. *Steady-State Performance with the Proposed Method and Conventional DTC and DFC Method*

Fig. 18 shows the experimental waveforms of current, torque and displacements at the speed of 1000 r/min when using two different methods [19]. The torque is calculated by (4) and outputted through a DA converter. On the one hand, the RMS current is reduced. In the conventional method, the RMS current is 369mA, yet the RMS current is 133mA in the proposed method. Then the torque-ampere ratio is increased with the proposed method. This is because the flux-linkage loop is removed and the current for flux-linkage amplitude control is none. On the other hand, it can be seen that the torque ripples with the proposed method and conventional method are 0.002N·m and 0.006N·m, respectively. One reason is that the flux-linkage loop is removed and the torque can be regulated more precisely, the other is that the voltage vectors tables are improved, and the commutation torque ripple is less with the proposed method. In addition, the displacements along α- and β-axes are similar with two methods in the experiment, and the maximum displacements are both about 25 μm.

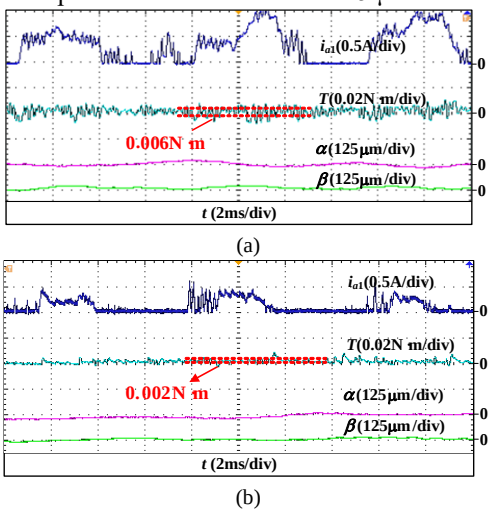

(a)

(b)

Fig. 18. Experimental waveforms of current, torque and displacements: (a) Conventional DTC and DFC. (b) Proposed method.

There are some reasons for the ripples and oscillations on the recorded currents and torques. Firstly, the time interval to update voltage vectors influences the current ripples, which is programmed in the DSP. Secondly, the used microprocessor is TMS320F2812, which does not have a FPU. Therefore, the current and torque are calculated by IQ module, which could decrease the accuracy of actual currents and torque. Thirdly, the inductance is changing in BSRMs due to variations of the rotor angular position and air-gap length. In order to generate the same levitation force, the required winding currents should be changed according to the levitation-force model. Moreover, there is a strong coupling between torque and levitation force, which also causes the torque ripple. Finally, sampling delays of devices and the sampling accuracy of current sensors could cause the ripples on the current and torque as well.

Fig. 19 shows the comparison of switching times with two different methods, where the typical current waveform and switching signals G_{a1} and G_{b1} are selected to count the number of switching times. The switching times of G_{a1} with the conventional method are 38 and that with the proposed method are only 20. Therefore, the switching loss with the proposed method can be reduced accordingly.

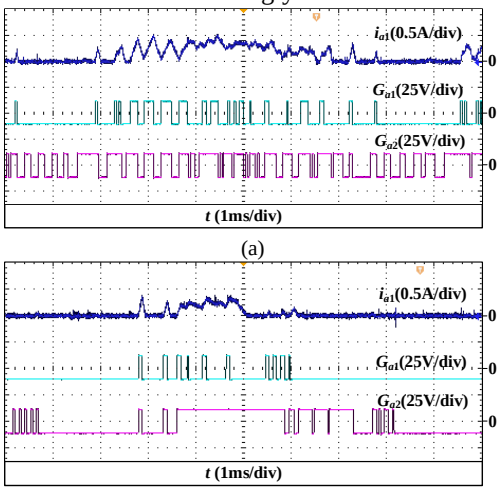

Fig. 19. Comparison of switching times: (a) Conventional DTC and DFC. (b) Proposed method.

The influence of levitation forces with two methods are shown in Fig. 20 [19]. It can be seen that the levitation force ripple is smaller with the proposed method under the condition of the same radial displacement ripples. This is because that the flux linkage is the control target as well in the conventional method, which could influence the selection of voltage vectors for levitation-force control and deteriorate the levitation-force tracking performance accordingly.

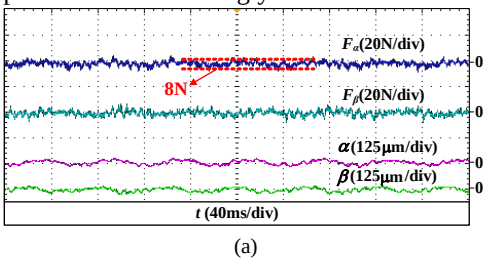

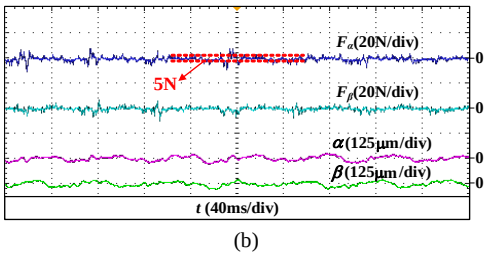

Fig. 20. Experimental results of the levitation forces: (a) Conventional DTC and DFC method. (b) Proposed method.

C. *Dynamic Performance of Speed Changing and Load Changing with Two Methods*

In order to test the dynamic performances of two methods, some experiments on speed changing and load changing are carried out. The motor speed is increased from 2000 r/min to 2500 r/min firstly and then decreased to 2000 r/min in the slope mode. The experimental waveforms are shown in Fig. 21. When the speed increases to 2500 r/min and decreases to 2000 r/min, the torque becomes the maximum and minimum values, respectively. Because the minimum value of torque is zero, the falling time of speed is more than its rising time. Moreover, it can be seen that the dynamic performances of two methods are similar from Fig. 21 (a) and Fig. 21 (b). This is because the reference maximum or minimum torque is the same with the two different methods. The radial displacement ripples also increase slightly when the speed changes. However, the motor can still achieve the stable levitation of rotor with the proposed method.

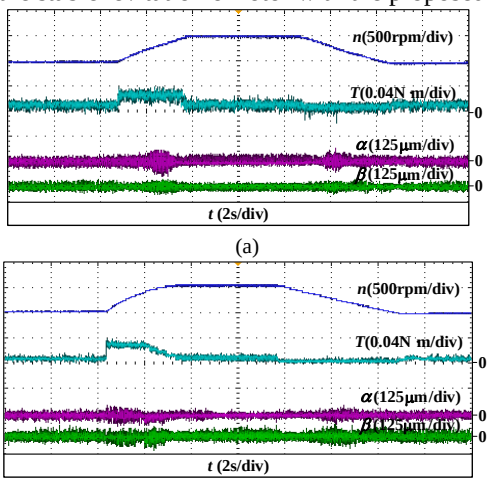

Fig. 21. Experimental results when speed increased from 2000 to 2500 r/min firstly and then decreased to 2000 r/min. (a) Conventional DTC and DFC. (b) Proposed method.

Fig. 22 shows the experimental results of load changing. It means the load increases suddenly at one moment and decreases at another moment. During the load-changing process, the sponge can be used to rub the rotor to increase the load torque. It can be seen that the speed and radial displacements keep unchanged with the two methods, which verifies the good dynamic performance of the conventional and proposed methods.

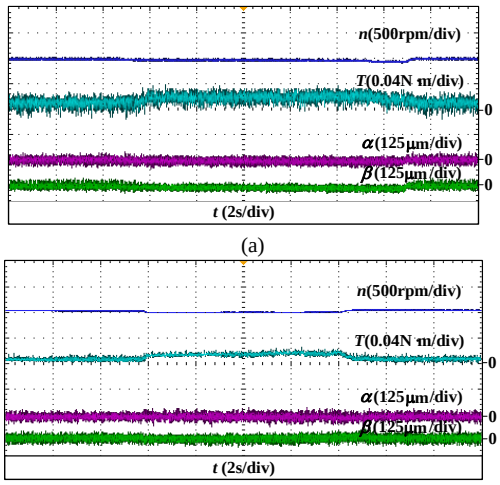

Fig. 22. Experimental results of load changing. (a) Conventional DTC and DFC. (b) Proposed method.

D. Dynamic Performance of Sudden Knock on the Shaft at Two Different Directions

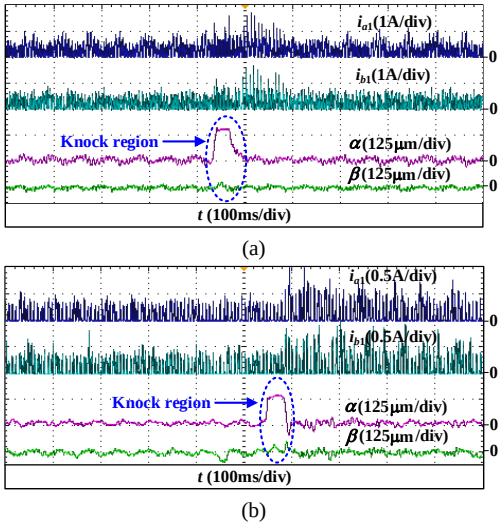

Fig. 23. Experimental results of sudden knocking along α-axis: (a) Conventional DTC and DFC. (b) Proposed method.

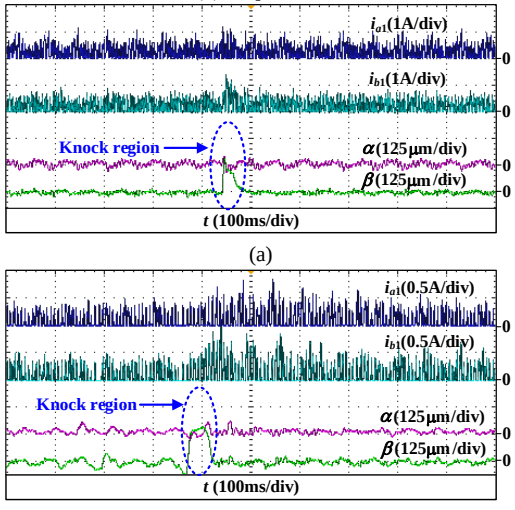

Fig. 24. Experimental results of sudden knocking along β-axis: (a) Conventional DTC and DFC. (b) Proposed method.

In order to test the dynamic characteristic of levitation forces, the experiments of a sudden knock on the shaft at two different directions are implemented as well. The hammer is used to knock the shaft during normal rotation of the motor. The experimental waveforms are shown in Fig. 23 and Fig. 24. When the shaft is knocked, it deviates to the opposite direction firstly but is pulled back immediately. Accordingly, the current increases at the moment of sudden knock to pull back the rotor. From Figs. 23 and 24, it is shown that the dynamic performances of levitation forces with two methods are similar.

E. Comparison Between the Proposed Method and Conventional DTC and DFC

In order to analyze the similarities and differences between the two control methods, the comparisons of some parameters are listed in Table VI when the motor is at the speed of 1000 r/min. Compared with the conventional method, the RMS current of phase A is reduced by 64% because the current is not conducted in the negative-torque region. Accordingly, the torque-ampere ratio is increased by 200% under the same load torque. Thirdly, the switching times in one electrical period of the proposed method are reduced by 47.3% as well. In addition, the torque ripple is also reduced by 66.7% compared with the conventional method, which also indicates that the torque is regulated better under the condition of the improved voltage vectors table and without the flux-linkage loop. For levitation, the control effect can be better with the proposed method in theory because the current of turn-off phase is dropped to zero. In other words, there is no extra levitation force of that phase in other time. However, the conventional DTC and DFC method adopts full-cycle current control, extra levitation forces may be produced in the regions of [-22.5°, -7.5°] and [7.5°, 22.5°] because four coil currents of that phase are not the same exactly, which can generate additional radial forces to deteriorate levitation control.

TABLE VI
COMPARISON BETWEEN THE CONVENTIONAL METHOD AND PROPOSED METHOD

	Conventional method	Proposed method
RMS current of phase A (mA)	369	133
Torque-ampere ratio (N·m/A)	0.01	0.03
Switching times in one electrical period	38	20
Torque ripple (N·m)	0.006	0.002
Levitation-force ripple (N)	8	5
Radial displacement (μm)	25	25

IV. CONCLUSION

This paper proposes an improved method based on direct torque control and direct force control for single-winding BSRMs. Different from the conventional DTC and DFC method, the proposed method removes the flux-linkage loop control and adds some voltage vectors, such as $v_7 \sim v_{12}$ and $-v_0 \sim -v_6$. On the one hand, the removal of the flux-linkage loop facilitates the torque control and improves the levitation-force tracking performance. Then the switching loss and torque ripple are

reduced accordingly. On the other hand, when the rotor moves to the inductance-descending region, the current can be shut off to prevent the generation of negative torque, which can decrease the RMS current and increase the torque-ampere ratio, and the winding copper loss can be reduced as well. Extensive simulations and experiments have been completed to verify the demonstrated performance.

REFERENCES

[1] A. Chiba, K. Kiyota, N. Hoshi, M. Takemoto, and S. Ogasawara, "Development of a rare-earth-free SR motor with high torque density for hybrid vehicles," *IEEE Trans. Energy Convers.*, vol. 30, no. 1, pp. 175–182, Mar. 2015.

[2] Z. Zhang, Z. Pian and G. Feng, "Research on new control model for switched reluctance motor," *2010 International Conference on Computer Application and System Modeling* (ICCASM 2010), Taiyuan, 2010, pp. V5-198-V5-202.

[3] J. F. Marques, J. O. Estima, N. S. Gameiro and A. J. Marques Cardoso, "A new diagnostic technique for real-time diagnosis of power converter faults in switched reluctance motor drives," *IEEE Trans. Ind. Appl.*, vol. 50, no. 3, pp. 1854-1860, May-Jun. 2014.

[4] S. Yao and W. Zhang, "A simple strategy for parameters identification of SRM direct instantaneous torque control," *IEEE Trans. Power Electron.*, vol. 33, no. 4, pp. 3622-3630, Apr. 2018.

[5] S. Song, L. Ge and M. Zhang, "Data-reconstruction-based modeling of SRM with few flux-linkage samples from torque-balanced measurement," *IEEE Trans. Energy Convers.*, vol. 31, no. 2, pp. 424-435, Jun. 2016.

[6] Z. Q. Zhu, B. Lee, L. Huang and W. Chu, "Contribution of current harmonics to average torque and torque ripple in switched reluctance machines," *IEEE Trans. on Magn.*, vol. 53, no. 3, pp. 1-9, Mar. 2017.

[7] H. Zhao, X. Cao and Z. Deng, "Position and radial displacement sensorless control method for bearingless switched reluctance motors," *Electrical Machines and Systems (ICEMS)*, Hangzhou, 2014, pp. 738-743.

[8] J. Zhou, Z. Deng, X. Cao, C. Liu and C. Liu, "Decoupling mechanism of torque and levitation-force control for 12/4 dual-winding bearingless switched reluctance motor," *Electrical Machines and Systems (ICEMS)*, Chiba, 2016, pp. 1-6.

[9] Y. Sun, X. Liu, D. Wang, J. Mao, "Extension of mathematical model to full angle for bearingless switched reluctance motors based on finite-element analysis," *Trans. China Electrotech.* Soc. 22 (9) (2007) 34–39 (in Chinese).

[10] A. Chiba, M. Rahman, T. Fukao, "Radial force in a bearingless reluctance motor, " *IEEE Trans. Magn.*, vol. 27, no. 2, pp. 786-790, Mar. 1991.

[11] A. Chiba, K. Chida, T. Fukao. Principles and characteristics of a reluctance motor with windings of magnetic bearing. *Proceedings of Power Electronics Conf.*, 1990, pp. 919-926.

[12] T. Fukao. The evolution of motor drive technologies: development of bearingless motors. *Proceedings of the Third Power Electronics and Motion Control Conf.*, 2000, pp. 33-38.

[13] W.-T. Liu and S.-M. Yang, "Modeling and control of a self-bearing switched reluctance motor," *Fourtieth IAS Annual Meeting. Conference Record of the 2005 Industry Applications Conf., 2005.*, Kowloon, Hong Kong, 2005, pp. 2720-2725.

[14] F. Lin and S. Yang, "Self-bearing control of a switched reluctance motor using sinusoidal currents," *IEEE Trans. Power Electron.*, vol. 22, no. 6, pp. 2518-2526, Nov. 2007.

[15] F. Ahmed, D. Saikia, S. Chatterjee, H. Singh, P. Das and K. Kalita, "Self-bearing switched reluctance motor: A review," *2012 1st International Conference on Power and Energy in NERIST (ICPEN)*, Nirjuli, 2012, pp. 1-6.

[16] M. Takemoto, A. Chiba and T. Fukao, "A method of determining the advanced angle of square-wave currents in a bearingless switched reluctance motor," *IEEE Trans. Ind. Appl.*, vol. 37, no. 6, pp. 1702-1709, Nov./Dec. 2001.

[17] X. Cao, Z. Deng, G. Yang and X. Wang, "Independent control of average torque and radial force in bearingless switched-reluctance motors with hybrid excitations," *IEEE Trans. Power Electron.*, vol. 24, no. 5, pp. 1376-1385, May 2009.

[18] Q. Sun, X. Cao and Z. Deng, "Direct torque and force control for dual-winding bearingless switched reluctance motor," *2014 17th International Conference on Electrical Machines and Systems (ICEMS)*, Hangzhou, 2014, pp. 1875-1880.

[19] X. Cao, J. Zhou, C. Liu and Z. Deng, "Advanced control method for a single-winding bearingless switched reluctance motor to reduce torque ripple and radial displacement," *IEEE Trans. Energy Convers.*, vol. 32, no. 4, pp. 1533-1543, Dec. 2017.

[20] M. Wang, "The fuzzy-PI control of switched reluctance motor based on DTC," *2009 International Conference on Measuring Technology and Mechatronics Automation*, Zhangjiajie, Hunan, 2009, pp. 606-609.

[21] A. D. Cheok and Y. Fukuda, "A new torque and flux control method for switched reluctance motor drives," *IEEE Trans. on Power Electron.*, vol. 17, no. 4, pp. 543-557, Jul. 2002.

[22] R. B. Inderka, R. W. De Doncker, "DITC-direct instantaneous torque control of switched reluctance drives," *IEEE Trans. on Ind. Appl.*, vol. 39, no. 4, pp. 1046-1051, Jul. 2003.

[23] X. Cao, H. Yang, L. Zhang and Z. Deng, "Compensation strategy of levitation forces for single-winding bearingless switched reluctance motor with one winding total short circuited," *IEEE Trans. Ind. Electron.*, vol. 63, no. 9, pp. 5534-5546, Sept. 2016.

[24] I. Takahashi and T. Noguchi, "A new quick-response and high-efficiency control strategy of an induction motor," *IEEE Trans. Ind. Appl.*, vol. IA-22, no. 5, pp. 820-827, Sept. 1986.

[25] N. Yan, X. Cao and Z. Deng, "Direct torque control for switched reluctance motor to obtain high torque–ampere ratio," *IEEE Trans. Ind. Electron.*, vol. 66, no. 7, pp. 5144-5152, Jul. 2019.

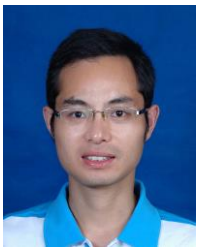

Zhenyang Hao received the B.Eng. degree from Nanjing Normal University, and the Ph.D. degree from Nanjing University of Aeronautics and Astronautics, Nanjing, China, in 2004 and 2010, respectively, both in Electrical Engineering.

Since 2010, he has been with Nanjing University of Aeronautics and Astronautics, where he is currently an Associate Professor at the Dept. of Electrical Engineering. From September 2014 to September 2015, he was a Visiting Scholar in Wisconsin Electric Machines and Power Electronics Consortium (WEMPEC), University of Wisconsin-Madison, U.S. His current research focuses on distributed generation and renewable energy, PMSM servo systems, and high speed machines.

Qiang Yu received the B.Eng. degree from Jiangsu University of Science and Technology, Zhenjiang, and the M.Sc. degree from Nanjing University of Aeronautics and Astronautics, Nanjing, China, in 2017 and 2020, respectively, both in Electrical Engineering. His current research focuses on bearingless switched reluctance motors.

Xin Cao (M'12) received the B.Eng., M.Sc., and Ph.D. degrees in electrical engineering from Nanjing University of Aeronautics and Astronautics, Nanjing, China, in 2003, 2006 and 2010, respectively.

Since 2011, he has been with Nanjing University of Aeronautics and Astronautics, where he is currently a Professor at the Dept. of Electrical Engineering. From June 2011 to September 2012, he was a Research Associate with the Dept. of Aeronautical and Automotive Engineering, Loughborough University, U.K. His current research focuses on distributed generation and renewable energy, switched reluctance machines, and high speed machines.

Xu Deng received the B.Eng. and M.Eng. degrees in Electrical Engineering from Nanjing University of Aeronautics and Astronautics, Nanjing, China, in 2010 and 2013, respectively. She received the PhD degree in Electrical Engineering from Newcastle University, Newcastle upon Tyne, U.K., in 2017.

She is currently a Research Associate of Electrical Power Research Group in the School of Engineering, Newcastle University, Newcastle upon Tyne, U.K. Her main researches are integrated drives and advanced control methods for power electronics and electric machines.

Xiang Shen received the Ph.D. degree in Mechanical Engineering from Queen Mary University of London, U.K., in 2017. He joined Newcastle University in the U.K. since 2018 to conduct multidisciplinary researches in mechanical design and thermal management on electric machines. In 2020, he became a Lecturer in Mechanical Engineering at Northumbria University, U.K., with research interests in mechanical design, thermal management, applied aerodynamics, wind engineering, aeroacoustics and multidisciplinary optimisation.